TECHNIQUE ARTICLE
Cytoskeleton, November 2013 70:718–728 (doi: 10.1002/cm.21138)
Published 2013 Wiley-Periodicals, Inc.†

Analysis of Flexural Rigidity of Actin Filaments Propelled by Surface Adsorbed Myosin Motors

Elina Bengtsson, Malin Persson, and Alf Månsson*

Faculty of Health and Life Sciences, Linnaeus University, Kalmar, Sweden

Received 26 April 2013; Revised 8 August 2013; Accepted 22 August 2013
Monitoring Editor: Laura Machesky

Actin filaments are central components of the cytoskeleton and the contractile machinery of muscle. The filaments are known to exist in a range of conformational states presumably with different flexural rigidity and thereby different persistence lengths. Our results analyze the approaches proposed previously to measure the persistence length from the statistics of the winding paths of actin filaments that are propelled by surface-adsorbed myosin motor fragments in the in vitro motility assay. Our results suggest that the persistence length of heavy meromyosin propelled actin filaments can be estimated with high accuracy and reproducibility using this approach provided that: (1) the in vitro motility assay experiments are designed to prevent bias in filament sliding directions, (2) at least 200 independent filament paths are studied, (3) the ratio between the sliding distance between measurements and the camera pixel-size is between 4 and 12, (4) the sliding distances between measurements is less than 50% of the expected persistence length, and (5) an appropriate cut-off value is chosen to exclude abrupt large angular changes in sliding direction that are complications, e.g., due to the presence of rigor heads. If the above precautions are taken the described method should be a useful routine part of in vitro motility assays thus expanding the amount of information to be gained from these.

Key Words: actin; cytoskeletal filament; Monte-Carlo simulations; molecular motor

*Address correspondence to: Alf Månsson, Faculty of Health and Life Sciences, Linnaeus University, SE-391 82 Kalmar, Sweden. E-mail: alf.mansson@lnu.se
Published online 4 October 2013 in Wiley Online Library (wileyonlinelibrary.com).

Introduction

Actin filaments are central components of the cytoskeleton that interact with numerous actin-binding proteins in executing their important roles in cell motility, cell-polarization, and other cellular activities [Pollard and Borisy, 2003; Chhabra and Higgs, 2007; Lindberg et al., 2008; Bugyi and Carlier, 2010; Galkin et al., 2012]. Actin is also a key component of the thin filaments in muscle. During muscle contraction, the thin filaments interact with arrays of myosin II molecular motors in the thick filaments of the sarcomere causing the thin and thick filaments to slide relative each other.

The actin filament can be described as composed of two right-handed helical proto-filaments that are wound around each other and where each protofilament consists of a chain of G-actin monomers [Kabsch et al., 1990; Oda et al., 2009; Hild et al., 2010]. Whereas this is the basic theme of the actin filament structure, several studies suggest that the actin filaments exist in a range of different structural states [Yanagida et al., 1984; Orlova and Egelman, 1993; Prochniewicz et al., 1993; Prochniewicz et al., 2004; Bugyi et al., 2006; Kozuka et al., 2006; Vikhorev et al., 2008a; Kupi et al., 2009; Tokuraku et al., 2009; Galkin et al., 2010, 2012], varying with respect to intra- and inter-monomer dynamics, the average helical twist of the filament etc. Furthermore, the equilibrium among the different states seems to vary with, e.g., tension in the filament [Uyeda et al., 2011; Galkin et al., 2012] as well as the presence of a range of actin binding proteins (including myosin) [Orlova and Egelman, 1993; Orlova et al., 1995; Bugyi et al., 2006; Kozuka et al., 2006; Vikhorev et al., 2008a; Kupi et al., 2009].

One way to probe for different structural actin filament states is by measuring the flexural rigidity (EI) of the actin filament [Yanagida et al., 1984; Gittes et al., 1993; Orlova and Egelman, 1993; Isambert et al., 1995; Bugyi et al., 2006]. Here, E is the Young's modulus of the filament and I is the second moment of inertia (proportional to the filament radius raised to the power of four). The flexural rigidity is most conveniently quantified by the persistence length $L_P = EI/kT$ where $1/kT$ is the Boltzmann factor. In practice, the

persistence length can be estimated from appropriate averages of the instantaneous shapes of a large number of fluorescence labeled actin filaments that are executing pseudo-two-dimensional thermal fluctuations between two cover-slips in solution [Yanagida et al., 1984; Gittes et al., 1993; Orlova and Egelman, 1993; Isambert et al., 1995]. However, an alternative approach [Vikhorev et al., 2008a] is to observe the winding paths of a large number of the filaments when they are propelled by myosin motors or heavy meromyosin (HMM) motor fragments adsorbed to a surface in the in vitro motility assay [Kron and Spudich, 1986; Kron et al., 1991]. Thus, we showed [Vikhorev et al., 2008a] theoretically [Duke et al., 1995] that the, so called, path persistence length of actin filaments in this assay should directly correspond to the filament persistence length. We also verified experimentally [Vikhorev et al., 2008a] that the path persistence length, estimated from the average change in tangent angle along the paths of HMM propelled actin filaments, is very similar to the persistence length estimated under similar conditions from images of filaments executing thermal fluctuations in solution. Further corroboration of this idea was recently obtained in measurements, using the two different approaches, of the persistence length of actin filament bundles cross-linked using the actin-binding protein fascin [Takatsuki et al., 2013]. Now, if there are several different meta-stable states of the actin filament (see above) [Yanagida et al., 1984; Orlova and Egelman, 1993; Orlova et al., 1995; Kozuka et al., 2006; Vikhorev et al., 2008a; Galkin et al., 2010] there may also be several different persistence lengths. It is not unlikely that the equilibrium between the states, and thereby the average persistence lengths, are altered for actin filaments with cardiomyopathy point mutations or for actin filaments that bind troponin or tropomyosin with such mutations. Therefore, persistence length measurements may contribute with important mechanistic insights into disease mechanisms. Moreover, the estimation of the actin filament persistence length from the filament paths give information about the effects of mutations on the actin filament when it interacts with myosin, of particular relevance, e.g., for cardiomyopathies. More generally, estimates of actin filament persistence length from filament paths adds to other relevant information obtained using an in vitro motility assay, transforming such assays further into high-content assays. Thus, importantly, a wide spectrum of information is obtained in one experiment and with limited amounts of proteins, e.g., as might be obtained in biopsies.

However, in order to make the assay generally useful for persistence length measurements, it is important to clarify methodological issues that may affect the results. This is the main purpose of the present paper. Our results, based on experiments and extensive Monte-Carlo simulations of actin filament paths [Nitta et al., 2006; Nitta et al., 2008; Månsson et al., 2012] suggest a robust approach for accurate and reproducible estimates of the persistence length of HMM propelled actin filament paths in the in vitro motility assay.

Results and Discussion

Experimental Conditions

We focus this article on the data analysis and only some key experimental complications (e.g., pixel-size) are studied systematically. However, some further experimental considerations deserve comments. First, it is essential to avoid formation of an anisotropic surface substrate for myosin motor adsorption [Vikhorev et al., 2008b]. Thus, it is important to avoid forming either topographically or chemically defined patterns on the surface as both may give rise to guiding of myosin propelled actin filament sliding in certain preferred directions [e.g., reviewed in Månsson, 2012]. We have found that trimethylchlorosilane (TMCS) derivatized surfaces [Sundberg et al., 2003; Albet-Torres et al., 2007; Månsson, 2012] are excellent for avoiding anisotropic surface substrates, showing generally great uniformity in chemistry and very low surface roughness. However, we have also performed experiments on nitrocellulose coated surfaces with seemingly similar results as on TMCS. Another issue to consider is self-organization of actin filaments that may arise on motility assay surfaces at high densities of actin filament [Kraikivski et al., 2006; Vikhorev et al., 2008b; Butt et al., 2010], e.g., if non-fluorescent blocking actin is used at high densities [Sundberg et al., 2003] to block pinning of actin filaments on rigor-like myosin heads [Homsher et al., 1992]. Such self-organization phenomena are essential to avoid as they encompass collective sliding of a large number of filaments along similar paths. Low incubation concentrations of blocking actin are important in this regard, particularly in the presence of methylcellulose. In an early study, we found that blocking actin concentrations of 1 μM or less [Sundberg et al., 2003] was sufficient to avoid problems also in the presence of methylcellulose and this is what we used here. Under these conditions, we observed no effect of methylcellulose on estimates of persistence length values [Vikhorev et al., 2008a]. Furthermore, we found (unpublished) similar persistence length values if blocking actin was omitted altogether. With regard to blocking actin, it is also important to consider the possible effect of phalloidin on the persistence length in relation to the fact that blocking actin filaments may anneal to the front end of a sliding filament [Vikhorev et al., 2008a]. If we study phalloidin-labeled actin filaments in the assay we therefore always also use phalloidin-labeled filaments for preparation of the non-fluorescent blocking actin and vice versa. Non-isotropic motor induced sliding, even if not detected by quick inspection of image sequences, is likely to lead to deviations of the cosine correlation function from a single exponential decay function. However, there may be other reasons for this (see below). Another way to detect anisotropy would be to plot a frequency distribution of all instantaneous angular sliding directions for all filaments studied. This distribution should be uniform in the range $[-\pi, \pi]$ radians.

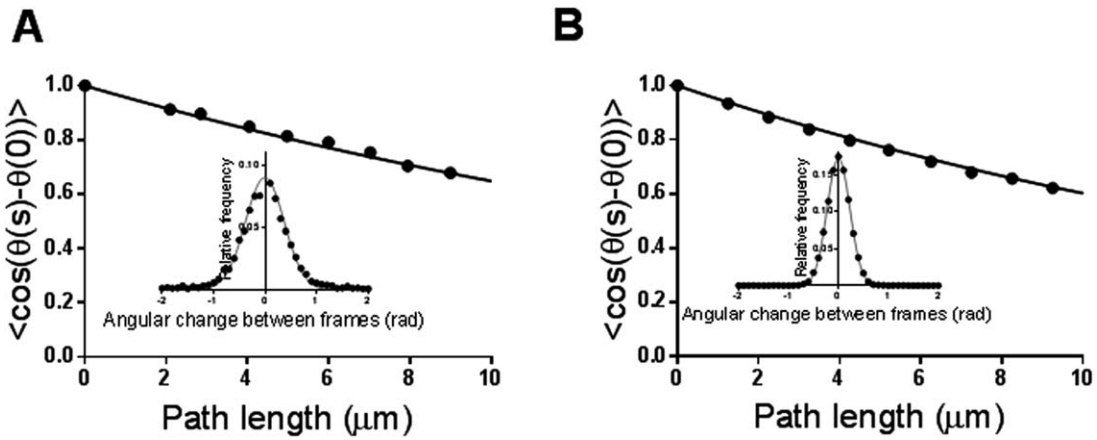

Fig. 1. Fit of single exponential decay function to the cosine correlation function where the latter is based on experimental or simulated data. (**A**) Experimental data (velocity: 9.27 ± 0.35 μm s^{-1}, mean ± 95% CI; frame rate 5 s^{-1}). (**B**) Simulated data (velocity: 10 μm·s^{-1}; frame rate 10 s^{-1}). *Insets*: Relative frequency distribution of angular changes between subsequent measurements.

It may often be of interest to perform experiments in the absence of phalloidin [Vikhorev et al., 2008a; Diensthuber et al., 2011]. In this case, the most convenient approach is to label the actin filaments by covalent attachment of fluorescent dyes. Previously, Vikhorev et al. [2008a] used *N*-hydroxysuccinimide (NHS)-rhodamine for this purpose with covalent attachment to the most reactive lysine(s) of 0.4 NHS-rhodamine per actin monomer on average. The lysine mediated coupling seems benign without appreciable effects on actin polymerization and actomyosin motor function [Kumar et al., 2012; Persson et al., 2013]. As an alternative to covalent functionalization, the actin filaments may also be visualized (and stabilized) by adding fluorescently labeled tropomyosin [Diensthuber et al., 2011]. A possible issue with experiments in the absence of phalloidin is the maintenance of the polymerized state. Importantly, however, previous results [Burlacu et al., 1992; Pavlov et al., 2007; Vikhorev et al., 2008a] suggest that this is not a real problem. For instance, Vikhorev et al. [2008] were able to observe actin filaments in the absence of phalloidin for >1 h after dilution to a concentration below that critical for polymerization.

The measurements of the actin filament persistence length from in vitro motility assay data rely on Eq. 1 for the decay of the CCF for polymers executing thermal fluctuations in two dimensions. If three-dimensional (3D) fluctuations are allowed, the exponent of Eq. 1 should be changed from $s/(2L_P)$ to s/L_P [Howard, 2001], i.e., for a given L_P the CCF would decay to $1/e$ for a lower value of s. The 3D case [Rivetti et al., 1996; Mucke et al., 2009] is of relevance for persistence length measurements using stationary filaments (e.g., on electrically charged glass surfaces [Arii and Hatori, 2008] or on electron microscopy grids [Orlova and Egelman, 1993]). Thus, as these filaments have executed thermal fluctuations in solution before deposition on the surface, the filament shape after surface biding may, in the case of strong surface–polymer interactions, represent a "trapped" projection of the 3D shape. This case is often associated with formation of surface loops and reduced apparent persistence length [Mucke et al., 2009]. In contrast, weak surface binding allows two-dimensional relaxation of filaments on the surface and calculation of the persistence length directly using Eq. 1 but with s taken as the distance along the filament.

Data Analysis

Monte-Carlo simulations were performed to analyze critical factors in path persistence length measurements. The simulations have appreciable advantages over experimental data for this purpose as an unambiguous theoretical persistence length (L_P^{theor}) can be defined. The similarity between simulated and experimental data based on 500 and 300 independent paths, respectively, are illustrated in Fig. 1. These data were simulated with $L_P^{theor} = 10$ μm, compared to experimental data with $L_P \approx 11.52 \pm 0.46$ μm (from fit of Eq. 1).

Before plotting of the CCF for the experimental data in Fig. 1, abrupt large changes in sliding direction (e.g., due to rigor heads), were removed as described in greater detail below. It can be seen that the CCF for both data sets are well fitted by an exponential function. Some variability of data around the exponential curve is attributed to the stochastic nature of the paths underlying the averages in the CCF. The good fit to the exponential function is consistent with the idea that only the first Gaussian term in Eq. 3 determines the update in sliding direction between analyzed frames. This is, of course, self-evident for the simulated data where the updates were drawn from a Gaussian distribution with standard deviation as in Eq. 1. However, importantly, for the experimental data, the results suggest that the tracking and analysis algorithm is effective in isolating the Gaussian component. Indeed it can be seen in the Gaussian fits of the experimental data (inset, Fig. 1A) that there are some anomalous large changes in sliding direction between measurements. The largest of these (>1.5 radians and <−1.5

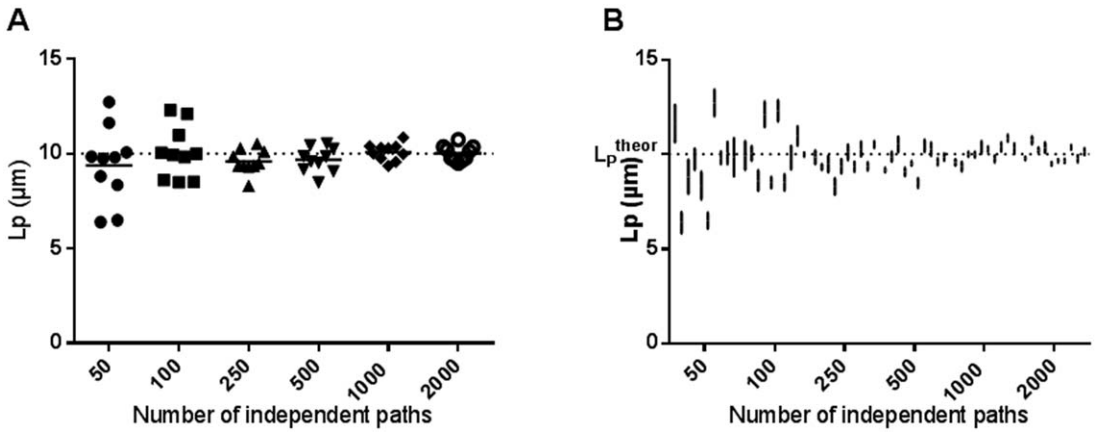

Fig. 2. Effect of number of independent filament paths on reproducibility in path persistence length estimates from single exponential fits to the CCF. Each data point represents a persistence length value obtained by exponential fit to the CCF for Monte-Carlo simulated data with the given number of independent paths. The underlying persistence length, L_P^{theor}, as a basis for all simulations was 10 μm. (**A**) Mean values for obtained persistence lengths at different numbers of independent paths. (**B**) 95% confidence intervals obtained in the non-linear regression single exponential fits for data presented in A.

radians) were eliminated by the analysis program before fitting the exponential function to the CCF (see further below).

We now performed simulations ($L_P^{theor} = 10$ μm) with different numbers of independent filament paths. This allowed us to test how many such paths are needed for accurate and reproducible determination of the persistence length, following the approach in the "Materials and Methods" section. Figure 2 shows estimates of path persistence lengths based on different numbers (in the range 50–2000) of simulated independent filament paths, each of 1 s duration (velocity 10 μm·s^{-1}). For each number of independent paths, 10 different simulations were performed and for each data set, L_P was obtained from an exponential fit to the CCF (Eq. 1). It can be seen in Fig. 2, that if more than about 200 and less than 1000 paths were followed, none of the 10 individual estimates for each given number of paths was different from L_P^{theor} by more than 1.8 μm. When 1000–2000 independent paths were studied, only two out of 10 individual estimates differed from L_P^{theor} by more than 0.5 μm. Data pooled over path length intervals of 1 or 0.5 μm were averaged and located in the midpoint of the interval in fitting the CCF. Virtually indistinguishable fits were obtained using the two different intervals (data not shown). We also tested whether the 95% CI for the exponential fit of the CCF could be used as indicator of the accuracy of the L_P determination. It is clear from Fig. 2B that the individual 95% CIs obtained in fits based on 100 or less independent paths only rarely (most certainly not in 95% of the cases) are wide enough to include also the true L_P. Therefore, the uncertainty in the estimates of L_P from few independent paths is considerably more substantial (Fig. 2A) than indicated by the 95% CI.

To summarize the requirements on the number of independent filament paths, this number should ideally be about 200 or greater. All analyses below follow this recommendation if not otherwise stated.

In experiments, errors are introduced in the estimate of the tangent angle along the filament path due to the finite pixel-sizes. This effect may become severe if the filament slides only a short distance compared to the pixel-size between two subsequent measurements, e.g., with large pixel-size, low velocity, high frame rates, or a combination of these factors. Errors may also be introduced if the sliding distance between subsequent frames is so long that the path curvature is truncated (Fig. 3A) [Homsher et al., 1992]. In order to elucidate these effects, simulations were performed using different combinations of velocity, pixel-size and time between frames as well as different pre-determined persistence lengths, L_P^{theor}. In Fig. 3B, we present simulated results for the case with low velocity (2.5 μm·s^{-1}) as seen e.g., at low MgATP concentrations or low temperature. We performed the simulations on the assumption of different pixel-sizes (0.02, 0.165, 0.33, and 0.66 μm/pixel) and a frame rate of 5 s^{-1}, corresponding to a sliding distance between analyzed frames of 0.5 μm. Thus, for the largest pixel-size, the simulated data points could end up in the same pixel for two consecutive frames, e.g., if the tangent angle of the filament path was 45% relative to the horizontal axis. Moreover, even for the second largest pixel-size the digitization error may be appreciable. These errors are reflected in the deviation of the cosine correlation function from a single exponential as illustrated in the simulated data in Fig. 3B. These deviations resulted in systematic errors in the persistence length estimated from single exponential fits (Fig. 3C). Thus, for the largest pixel-sizes we found either erroneously low (for the case with 0.33 μm pixel-size) or high (for 0.66 μm pixel-size) persistence length due to this complication. The basis, in the shape of the CCF, for these effects is clear from Fig. 3B. The pixel-size is not necessarily possible to modify in a given experimental set-up. On the other hand, as indicated above, the important parameter is not the pixel-size per se but rather the ratio $v_f\Delta t$/pixel-size.

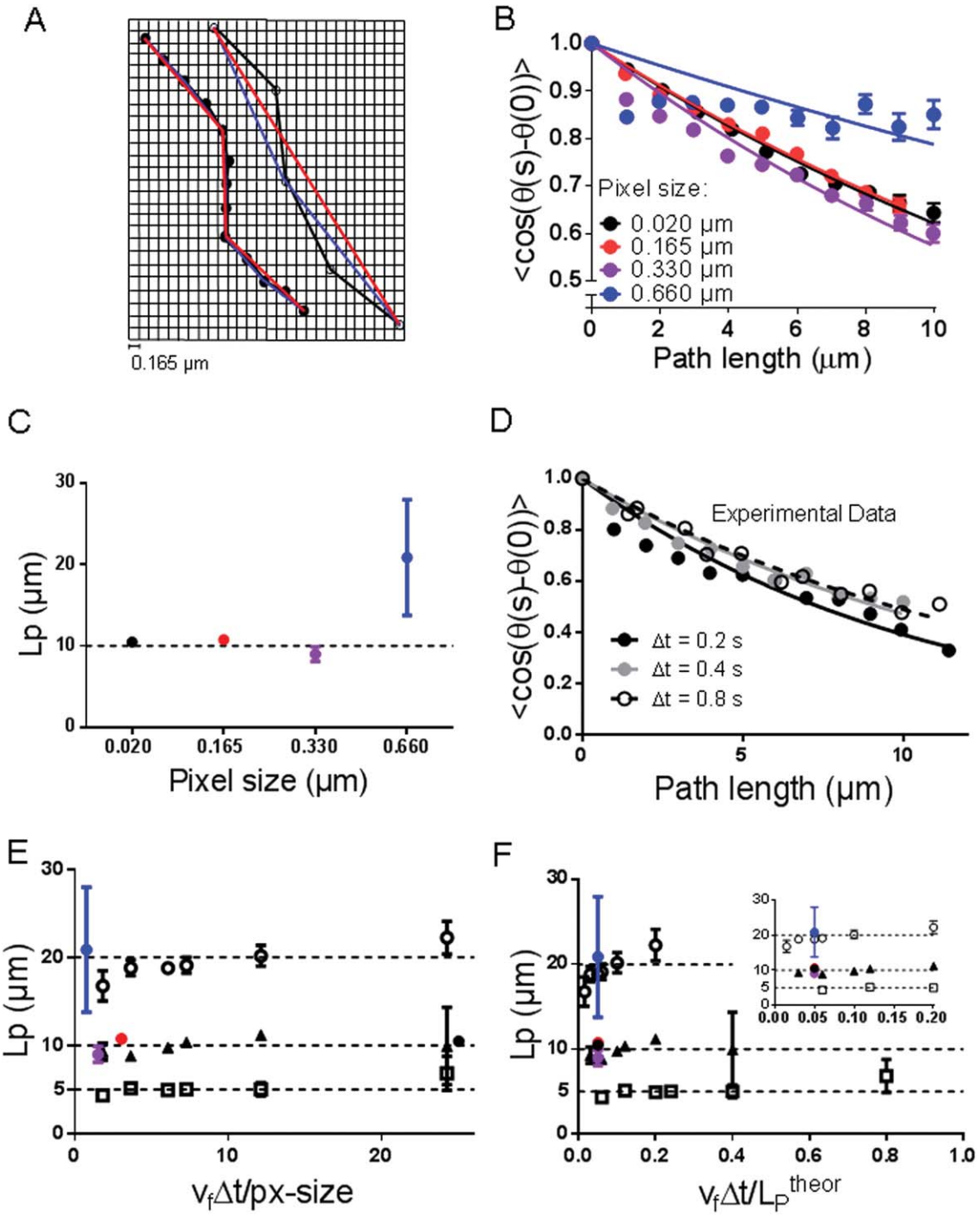

Fig. 3. Digitization effects. (**A**) Illustration of truncation effects when analyzing a given filament path at different frame rates. The circles indicate observed filament positions when sliding at 3 µm·s^{-1} (filled circles) and 10 µm·s^{-1} (open circles), and the black, blue and red lines indicate apparent filament paths for 0.1, 0.2, and 0.4 s between analyzed frames, respectively. Each square in the grid corresponds to a pixel. (**B**) Simulated data. Fit of the CCF based on simulated data at different pixel-sizes to the exponential function (Eq. 1). The simulations of filament paths at low velocity (2.5 µm·s^{-1}) show changes in estimated persistence length value as a complication due to digitization effects related to finite pixel-size. The filaments were assumed to move 0.5 µm between analyzed frames (i.e., frame rate of 5 s^{-1}). (**C**) Estimated persistence lengths (±95% CI) from the fits in B to simulated data, with the dashed line illustrating the theoretical persistence length (L_P^{theor}). Same color code as in B. (**D**) Fit of exponential function to CCF for experimental data with different time intervals between analyzed frames. In this experiment blocking actin was omitted, the pixel-size was 0.165^2 µm^2 and [MgATP] = 0.05 mM to reduce velocity (2.26 ± 0.04 µm·s^{-1}; mean ± 95% CI, number of filaments (n_f) 114). Finally, the persistence length was determined to 6.99 ± 0.57 µm (mean ± 95% CI), using 0.8 s between analyzed frames. The number of independent filament paths was 100 at 0.8 s. Note, the same experimental data was used just employing different time intervals between frames. (**E**) Effect of ratio $v_f\Delta t$/pixel-size on estimated persistence length. Simulated data. Open circles: L_P^{theor} = 20 µm, filled symbols: L_P^{theor} = 10 µm, included data from B to C (i.e., constant $v_f\Delta t$, same color code as in B and C), open squares: L_P^{theor} = 5 µm, L_P^{theor} illustrated with dashed lines. (F) Effect of $v_f\Delta t$ on estimated persistence length in relation to underlying theoretical persistence length (L_P^{theor}). Same data as in E.

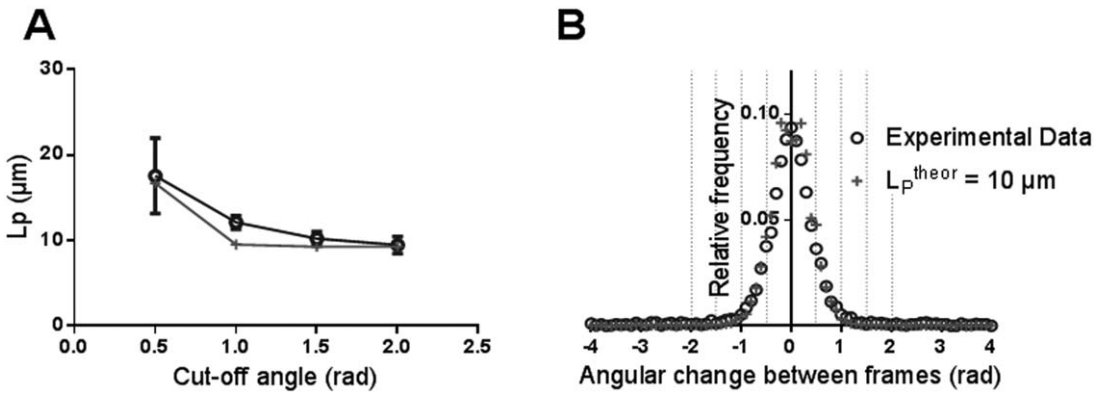

Fig. 4. Cut-off angle. (**A**) L_P values for simulated (10 μm·s^{-1}; n_f = 200).and experimental data (velocity; 7.68 ± 0.26 μm·s^{-1}, mean ± 95% CI, n_f = 148) where different cut-off values for $\Delta\theta(s)$ are used. Experimental data (circles) along with simulations (grey plus sign) representing one flexibility state (L_P^{theor} = 10 μm) of the actin filament. (**B**) Frequency distribution of angular changes between subsequent analyzed frames (frame rate 5 s^{-1}). Dashed vertical lines at cut-off values tested.

In one set of experiments we reduced this ratio by reducing v_f as result of lowering [MgATP] to 0.05 mM. It is clear from Fig. 3D that this also reduced L_P (to 6.99 ± 0.57 μm) an issue that is briefly discussed below. More importantly, however, with the present methodological focus, we illustrate in Fig. 3D how changed Δt, associated with changed $v_f\Delta t$/pixel-size ratio, led to altered shape of the cosine correlation function. It is shown that the deviation from the exponential function is appreciably reduced by increasing Δt to compensate for the reduction in v_f. A more extensive analysis of the effect of altering the ratio $v_f\Delta t$/pixel-size is depicted in Fig. 3E on basis of simulated data. It can be seen here that the exponential fit to the CCF gives an accurate estimate of the underlying L_P^{theor} if the ratio $v_f\Delta t$/pixel-size is held within the rather wide range between 4 and 12 for the entire range of experimentally reasonable persistence lengths (5–20 μm). For lower values than 4, there are risks of digitization errors of the type illustrated in Figs. 3B and 3C. At higher values than 12, truncation effects of the type illustrated in Fig. 3A may affect the estimate of the L_P-value. It is also indicated in Fig. 3E that high path persistence lengths (L_P^{theor}) increase the sensitivity to digitization errors. This can be understood on basis of the straighter paths in this case. For instance, consider a filament sliding with a very small positive tangent angle related to the horizontal axis and initially projected onto the lower part of a given row of pixels. It is clear that this filament will be projected for longer time onto the same pixel row the higher the path persistence length, i.e., the longer sliding distance that is, on average, required before an appreciable change in sliding direction is expected.

It was initially surprising to note that the truncation of the filament path (Fig. 3A), seen if $v_f\Delta t$ is large compared to L_P does not seem to cause serious errors in the estimate of the persistence length. This finding is even clearer from Fig. 3F where it can be seen that increases in $v_f\Delta t$ up to 50% of L_P^{theor} had negligible effect on the estimated path persistence length value. This finding can be understood by inspecting Fig. 3A where it can be seen that chords drawn between different points along the filament path (with different separation between them) all are characterized by angles relative to a given axis that are very similar to tangent angles of the filament paths close to the midpoint between the two chord-ends on the filament

To summarize, the results in Fig. 3 suggest that, for accurate determination of the persistence length, it is important that 4 × pixel-size < $v_f\Delta t$ and, furthermore, that $v_f\Delta t$ <0.5 × L_P and <12 × pixel-size.

One issue that was not explicitly considered in the analysis above is the exclusion of abrupt direction changes [Vikhorev et al., 2008a], i.e., instantaneous angular changes greater than a certain cut-off value. These abrupt changes in direction may occur in experiments, e.g., due to the presence of rigor heads. The abrupt changes may also be simulated but this was not done in the above analysis. However, in the analysis, we nevertheless used a cut-off value of 1.5 radians for all analyzed data. The reason for excluding the abrupt direction changes is that they are assumed not to be sampled from an angular distribution that is due to thermal fluctuations of the leading end of the filament [Duke et al., 1995]. Instead, we attribute them mainly to pinning of the actin filaments on rigor myosin heads in the in vitro motility assay [Vikhorev et al., 2008b]. However, for high $v_f\Delta t/L_P$ ratio (Fig. 2), the choice of the cut-off value may introduce systematic overestimation of the persistence length by removing the filaments with the most curved paths from the analysis. Importantly, however, the data in Fig. 3F shows that any such effect is negligible with the cut-off value routinely used here, particularly as the error due to path truncation at large $v_f\Delta t/L_P$ ratio (see above) would operate in the same direction as the effect of the cut-off. Nevertheless, it was of interest to examine how the introduction of the cut-off value influenced the estimate of the persistence length. To this end, we tested a number of different cut-off values, both for experimental data and

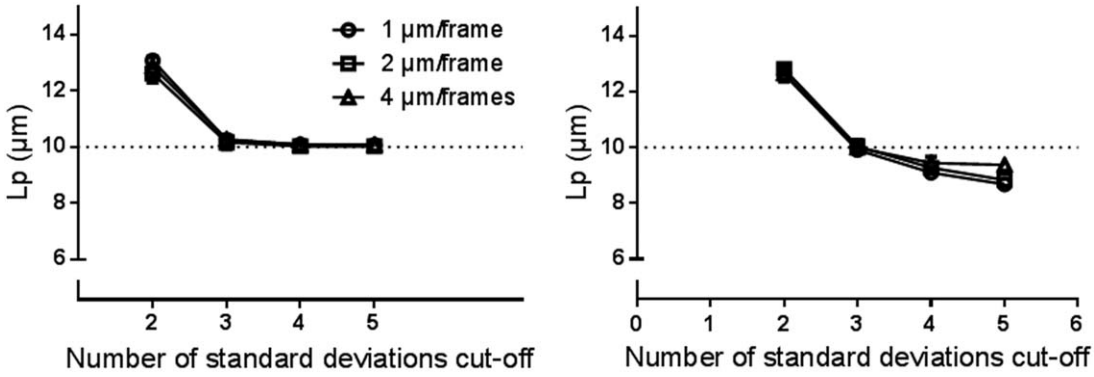

Fig. 5. Effects of cut-off angle and sliding distance between measurements. (**A**) Cut-off values given in terms of the number of standard deviations for simulations without uniform random errors. (**B**) Same analysis as in A but with uniform random errors in about 2.5% of the updates of the sliding direction between subsequent measurement points along a filament path. Digitization effects considered neither in A nor in B. Theoretical persistence length in simulations, 10 µm.

simulations (Fig. 4A). It can be seen in Fig. 4 that the dependence of the experimental data on the cut-off value closely mimics the results of Monte-Carlo simulations assuming one single population of actin filaments having a persistence length of ~10 µm. This is also consistent with the well superimposed frequency distributions of the angular change between measurements for the experimental and simulated data (Fig. 4B).

A more detailed analysis was also performed of the effect of the cut-off angle on the final outcome of the analysis. The relevant scale in this case was the standard deviation (given by Eq. 2; see below), i.e., for a range of conditions, we plot estimated persistence lengths against different cut-off values expressed in terms of the number of standard deviations. Data in Fig. 5 are based on simulated results for three different sliding distances between image frames, i.e., for three different ratios $v_f\Delta t/L_P^{theor}$. In Fig. 5A, no abrupt changes in sliding direction are assumed. Data in Fig. 5B include such abrupt simulated changes, as described in "Materials and Methods" section. It can be seen from Fig. 5A that, in the absence of abrupt changes, the cut-off value should be larger than $3SD=3\sqrt{v_f\Delta t/L_P^{theor}}$ (Eq. 2) as lower cut-off values lead to overestimated L_P-values due to elimination of the most curved filament paths from the analysis. The data in Fig. 5B, including abrupt changes in <2.5% of the updates of the sliding directions between data points, would clearly benefit from as low cut-off value as possible close to 3SD in order to prevent the abrupt changes to cause an underestimation of the persistence length. However, it is also clear that only a small error (less than ~1 µm) is introduced if the cut-off value is in the range of 3–5 standard deviations.

A comparison of the data in Figs. 5 and 4, where $SD=\sqrt{v_f\Delta t/L_P^{theor}}$ was about 0.39, indicates that the experimental data are affected by abrupt large changes in sliding direction. If the latter are taken into account it seems clear that the use of a cut-off of 1.5 radians (corresponding to 3.8 SD) leads to underestimation of the persistence length. Generally, it seems to be useful to plot the estimated L_P against the cut-off value, expressed in terms of SD, to judge the effects of abrupt angular changes. Otherwise, from a practical point of view it seems reasonable (cf. Figs. 5A and 5B) to select the cut-off in the range between 3 and 4 SDs.

Analysis of persistence length data is subject to several complexities, whether the measurements are based on observations of motor propelled filaments in the in vitro motility assay or thermally fluctuating filaments in solution. In this connection one may first consider our experimental persistence length of ~11.65 µm that is lower than the most frequently reported values for phalloidin labeled actin filaments (15–18 µm) [Yanagida et al., 1984; Gittes et al., 1993; Ott et al., 1993; Isambert et al., 1995; Yasuda et al., 1996; Greenberg et al., 2008; Vikhorev et al., 2008a]. This is probably related to findings [Yanagida et al., 1984; Nitta et al., 2008; Vikhorev et al., 2008a] that the persistence length is reduced by binding of myosin motor fragments to phalloidin labeled actin filaments [Yanagida et al., 1984; Orlova and Egelman, 1993; Vikhorev et al., 2008a]. Whereas the effect was rather small at the ionic strength used here [Vikhorev et al., 2008a] it is also important to note that subtle differences in polymerization conditions [Steinmetz et al., 1997] may produce actin filaments with varying flexibility. This is consistent with a rather low persistence length also in solution (12.61 ± 0.65 µm) in this study.

Another source of complexity worth considering is length dependent persistence length characteristic of certain versions of so called worm-like bundle model [Heussinger et al., 2010]. This type of behavior may be attributed to domination on different length scales of either homogeneous rod bending motions or shearing movements of monomers or cross-linking components relative to each other. The behavior has been experimentally demonstrated

[Pampaloni et al., 2006] and been proposed to explain the short persistence length (~100 μm) measured from the path of kinesin propelled microtubules [Nitta et al., 2008; Van den Heuvel et al., 2008] compared to >1 mm for long microtubules based on thermal fluctuations in solution [Gittes et al., 1993]. In contrast to the different persistence length estimates for microtubules in solution and when propelled by motors on surfaces, no consistent differences of similar type have been observed for fascin–actin bundles [Takatsuki et al., 2013]. For isolated actin filaments, effects of this type are not expected.

As originally suggested in Duke et al. [1995], the persistence length of motor propelled filament paths may be assumed to be determined by thermal fluctuations of the leading end of the filament and thus by the persistence length (materials properties) of this filament part. Generally, the rest of the filament is assumed to have the same persistence length as the leading end and thus trace out the same path as the latter. However, this may not always be the case, e.g., due to different structural states along a filament or with HMM propelled actin bundles (e.g., fascin–actin bundles) [Ishikawa et al., 2003; Takatsuki et al., 2010] with different number of cross-linked filaments along the bundle length. In the latter case, the central segment of the bundle may be expected [*cf.* Ishikawa et al., 2003] to have higher rigidity than the front segment and thereby dominate in determining the sliding direction. Thus, a rigid bundle segment propelled by a large number of motors would not readily follow the path devised by a more flexible region at the front.

A final complication to consider is the possible effect of side-ways movement of motor propelled cytoskeletal filaments that may be produced by motor induced torques. The potential existence of this type of effects was indicated by consistently counterclockwise curved paths of actin filaments propelled by myosin 1c motors adsorbed to supported lipid bilayers [Pyrpassopoulos et al., 2012]. While, the importance is uncertain for other surface-motor-filament combinations, the possibility of motor-induced sideways movements should be kept in mind. In this connection, it is important to consider the effect of lowered MgATP concentration on HMM propulsion of actin filaments. The reduced MgATP concentration both increases the fraction of the cycle time and the absolute time that the myosin heads spend attached to actin (thereby also increasing the number of attached heads at a given time). Any of these effects, or a combination of them, may explain the apparent reduction in the actin filament persistence length with reduced [MgATP] (Fig. 3D), either by affecting the filament structure (materials properties) or by imposing increased torque impulses randomly for clockwise or counterclockwise turning of the filament tip. These effects are interesting and deserve further investigations. However, due to the complexity of the phenomenon, such investigations are outside the scope of this study.

In contrast to the reduced velocity at lowered MgATP concentration (that selectively reduces the cross-bridge detachment rate) the reduced velocity at lowered temperature (reducing both cross-bridge detachment and attachment rates) was not associated with any significant effects on the path persistence length [Vikhorev et al., 2008a]

Conclusions and Perspectives

Our results show that the persistence length of HMM propelled actin filaments may be estimated with high accuracy and reproducibility from the statistics of the winding paths of heavy meromyosin propelled actin filaments. For best performance, it is important: (1) to design the in vitro motility assay experiments appropriately as discussed above, (2) to choose experimental conditions such that four times the pixel-size is less than $v_f \Delta t$ which is less than 12 times the pixel-size and less than 0.5 times the smallest expected persistence length value, (3) to include at least 200 independent filament paths in the analysis, and (4) to use a cut-off value corresponding to 3–4 times the lowest value of $SD = \sqrt{v_f \Delta t / L_P^{theor}}$ expected. Moreover, in order to test the appropriateness of the chosen cut-off value it may be useful to plot the estimated L_P value for varied cut-off values. Finally, we have highlighted complexities that are important to keep in mind when interpreting persistence length data obtained using the present approach.

This method to estimate the path persistence length should be readily made a routine part of in vitro motility assays thus expanding the amount of information to be gained from these. This may be of value to characterize functional changes in the actomyosin system introduced by various point mutations and would contribute to elucidating the possible role of structural changes in the actin filament in regulation [Egelman and Orlova, 1995; Kozuka et al., 2007] and/or actomyosin based force-generation [Yanagida et al., 1984; Kozuka et al., 2006].

Materials and Methods

Protein Preparations, Surface Preparations, and In Vitro Motility Assays

Myosin was isolated from fast skeletal muscle [Klinth et al., 2003] followed by preparation of heavy meromyosin (HMM) using tosyl-lysine chloromethyl ketone (TLCK) treated chymotrypsin. Actin was prepared from acetone powder [Pardee and Spudich, 1982]. Polymerization into actin filaments was achieved by adding KCl (50 mM) and $MgCl_2$ (2 mM) to G-actin in a G-buffer of the following composition: 2 mM Tris base, 0.2 mM magnesium adenosine-5′-triphosphate (MgATP), 0.5 mM dithiothreitol (DTT), 0.2 mM $CaCl_2$, 3 mM NaN_3. Aliquots of F-actin were subsequently frozen in liquid nitrogen and stored at −80°C [Balaz and Mansson, 2005]. For phalloidin

labeling, the actin filaments were treated overnight with tetramethylrhodamine isothiocyanate phalloidin (TRITC-Ph) or non-fluorescent phalloidin (Ph) at 50% molar excess (on actin monomer basis).

In vitro motility assays were performed using cover-slips that were functionalized with trimethylchlorosilane (TMCS) [Sundberg et al., 2003] for HMM absorption. All proteins were diluted in Buffer A [10 mM 3-(*N*-morpholino)propanesulfonic acid (MOPS), 1 mM $MgCl_2$, 0.1 mM potassium ethylene glycol tetraacetic acid (K_2EGTA), 1 mM DTT, and 50 mM KCl] Flow cells with TMCS-derivatized surfaces were first incubated with HMM (120 or 40 μg mL^{-1}) for 2 min and subsequently with bovine serum albumin (BSA; 1 mg·mL^{-1}) for 30 s. The ATP insensitive "rigor heads" of HMM were blocked by incubating non-fluorescent Ph labeled actin filaments for one minute before the flow cell was washed using Buffer B (10 mM MOPS, 1 mM $MgCl_2$, 0.1 mM K_2EGTA, 10 mM DTT, 25 mM KCl, 3 mg·mL^{-1} glucose, 20 U mL^{-1} glucose oxidase, 460 U·mL^{-1} catalase, and 1 mM MgATP). This was followed by a second wash with Buffer A. The TRITC-Ph labeled actin filaments were subsequently added to the flow cell and incubated for 30 s, followed by rinsing with Buffer A. Finally the assay solution was added. The assay solution was based on Buffer B but with an ionic strength of 130 mM by addition of appropriate amounts of KCl. Moreover, the assay solution contained 2.5 mM creatine phosphate, 56 U·mL^{-1} creatine kinase and 0.64% methylcellulose.

The image sequences for analysis of motility assays were obtained using a Nikon Eclipse TE300 inverted microscope (Nikon, Tokyo, Japan) with epi-fluorescence illumination and a temperature regulated oil immersion Nikon 100×, 1.4 NA objective. The image sequences were recorded using an EM-CCD-camera (Hamamatsu, C9100) at frame rates of 5–10 s^{-1} as appropriate and with a pixel magnification of 0.165 × 0.165 μm^2 per pixel.

Persistence Length of Actin Filament Paths

Actin filaments in the in vitro motility assay were randomly selected for tracking and analysis. Filaments that were clearly pinned on non-functional, rigor-like myosin heads or that were initially located closer to the image edge than 20 μm were excluded already in the tracking process. The persistence length of the filament paths were obtained from plots of a cosine correlation function, $<\cos[\theta(s) - \theta(0)]>$, against the distance ($s$) along the filament paths. In this case, s and $\theta(s)$ (the tangent angle at s) were obtained from coordinates obtained by manual tracking (using the computer pointer device) of the leading end of the filament at 0.1–0.8 s time intervals (depending on average sliding velocity). The tracking, as well as the subsequent calculation of the filament path length and the angle $\theta(s)$, was achieved using Matlab (MathWorks, Natick, MA) according to previously described principles [Vikhorev et al., 2008a]. On the assumption that the instantaneous changes in filament sliding direction were independent, we sometimes obtained several paths for analyses from a given filament. These different paths were assumed to be independent. For instance, a filament that could be observed sliding for more than 40 μm gave rise to 4 "independent" 10 μm paths.

The analysis algorithm that was run subsequent to tracking was designed to interrupt the analysis of a filament path if large and abrupt changes occurred in the sliding direction (e.g., due to the presence of occasional rigor heads). The appropriate definition of the cut-off angle defining an "abrupt change" in sliding direction was (unless otherwise stated) here taken as 1.5 radians, approximately 3–5 times the standard deviation of the angular change ($\Delta\theta$) in sliding direction between subsequent tracking points. This cut-off value was higher than in previous work [Vikhorev et al., 2008a]. The effects of choosing certain cut-off values are analyzed in some detail above.

After the tracking and initial processing, the persistence length (L_P) was obtained from fits of an exponential function to the cosine correlation function (CCF; $<\cos[\theta(s) - \theta(0)]>$) calculated from the experimental data:

$$<\cos(\theta(s)-\theta(0))> = \exp(-s/[2L_P]) \quad (1)$$

Before fitting, data were pooled for path length intervals of 1 or 0.5 μm and the mean values of the cosine correlation function in these intervals (located in the midpoint of the interval) were used.

Monte-Carlo Simulations

Actin filament paths in the in vitro motility assay were simulated in Matlab, using a Monte-Carlo approach [Nitta et al., 2006; Nitta et al., 2008; Månsson et al., 2012). The random path was created by updating the sliding direction at defined short time intervals (Δt) with an angular change ($\Delta\theta_{therm}$) from a Gaussian distribution with zero mean value and a standard deviation [Nitta et al., 2008]:

$$SD = \sqrt{\frac{v_f \Delta t}{L_P^{theor}}} \quad (2)$$

Here L_P^{theor} is the theoretical persistence length of the simulated path. The Matlab random number generator for a normal distribution (random) was used in this step. The distance that a "filament" moved between subsequent updates in sliding direction was given by the product of Δt and the velocity (v_f). For evaluation of digitization effects, different pixel-sizes were simulated. In this case, the simulated coordinates of the filament were shifted to the centre of the pixel in the output.

Possible effects of uniform random noise (e.g., due to abrupt changes in sliding direction imposed by rigor-like heads) were included in the simulations by updating the

sliding direction ($\Delta\theta$) using two components. One of these was due to thermal fluctuations of the leading tip of the filaments ($\Delta\theta_{therm}$), simulated as described above. The second component was an abrupt change ($\Delta\theta_{uni}$), possibly due to "pinning" of the filament on rigor-like cross-bridges. That is:

$$\Delta\theta = \Delta\theta_{therm} + \Delta\theta_{uni} \quad (3)$$

For each update the first term was obtained as described above. The second term, $\Delta\theta_{uni}$, was set to zero in 97.5% of the cases (randomly determined) and drawn from the range $[-\pi, \pi]$ radians, assuming a uniform probability distribution, in 2.5% of the cases.

The simulated filament paths, including complications as above, were used as a basis for obtaining cosine correlation functions. Persistence lengths were then obtained by exponential fits as described in detail for experimental data (Eq. 1).

Statistical Analysis Including Non-linear Regression

Non-linear regression and statistical analyses were performed using GraphPad Prism (GraphPad Software, 6.00 for Windows, San Diego, CA). Because the number of data points decreased and the variance increased for higher values of *s*, the CCF was fitted to the mean values for each *s* without consideration of the experimental variability and the number of underlying measurements at the given *s*-value. Data are given as mean ± 95% confidence interval (CI) unless otherwise stated.

Acknowledgments

This study was funded by The Swedish Research Council (Project # 621-2010-5146), The Carl Trygger Foundation, The Crafoord Foundation and the Faculty of Natural Sciences and Engineering and the Faculty of Health and Life Sciences at Linnaeus University.

References

Albet-Torres N, O'Mahony J, Charlton C, Balaz M, Lisboa P, Aastrup T, Mansson A, Nicholls IA. 2007. Mode of heavy meromyosin adsorption and motor function correlated with surface hydrophobicity and charge. Langmuir 23(22):11147–11156.

Arii Y, Hatori K. 2008. Relationship between the flexibility and the motility of actin filaments: effects of pH. Biochem Biophys Res Commun 371(4):772–776.

Balaz M, Mansson A. 2005. Detection of small differences in actomyosin function using actin labeled with different phalloidin conjugates. Anal Biochem 338(2):224–236.

Bugyi B, Carlier MF. 2010. Control of actin filament treadmilling in cell motility. Annu Rev Biophys 39:449–470.

Bugyi B, Papp G, Hild G, Lorinczy D, Nevalainen EM, Lappalainen P, Somogyi B, Nyitrai M. 2006. Formins regulate actin filament flexibility through long range allosteric interactions. J Biol Chem 281(16):10727–10736.

Burlacu S, Janmey PA, Borejdo J. 1992. Distribution of actin filament lengths measured by fluorescence microscopy. Am J Physiol 262(3 Pt 1):C569–C577.

Butt T, Mufti T, Humayun A, Rosenthal PB, Khan S, Molloy JE. 2010. Myosin motors drive long range alignment of actin filaments. J Biol Chem 285(7):4964–4974.

Chhabra ES, Higgs HN. 2007. The many faces of actin: matching assembly factors with cellular structures. Nat Cell Biol 9(10):1110–1121.

Diensthuber RP, Muller M, Heissler SM, Taft MH, Chizhov I, Manstein DJ. 2011. Phalloidin perturbs the interaction of human non-muscle myosin isoforms 2A and 2C1 with F-actin. FEBS Lett 585(5):767–771.

Duke T, Holy TE, Leibler S. 1995. Gliding assays for motor proteins: a theoretical-analysis. Phys Rev Lett 74(2):330–333.

Egelman EH, Orlova A. 1995. New insights into actin filament dynamics. Curr Opin Struct Biol 5(2):172–180.

Galkin VE, Orlova A, Egelman EH. 2012. Actin filaments as tension sensors. Curr Biol 22(3):R96–R101.

Galkin VE, Orlova A, Schroder GF, Egelman EH. 2010. Structural polymorphism in F-actin. Nat Struct Mol Biol 17(11):1318–1323.

Gittes F, Mickey B, Nettleton J, Howard J. 1993. Flexural rigidity of microtubules and actin-filaments measured from thermal fluctuations in shape. J Cell Biol 120(4):923–934.

Greenberg MJ, Wang CL, Lehman W, Moore JR. 2008. Modulation of actin mechanics by caldesmon and tropomyosin. Cell Motil Cytoskeleton 65(2):156–164.

Heussinger C, Schuller F, Frey E. 2010. Statics and dynamics of the wormlike bundle model. Phys Rev E: Stat NonlinearSoft Matter Phys 81(2 Pt 1):021904.

Hild G, Bugyi B, Nyitrai M. 2010. Conformational dynamics of actin: effectors and implications for biological function. Cytoskeleton 67(10):609–629.

Homsher E, Wang F, Sellers JR. 1992. Factors affecting movement of F-actin filaments propelled by skeletal muscle heavy meromyosin. Am J Physiol 262(3 Pt 1):C714–C723.

Howard J. 2001. Mechanics of Motor Proteins and the Cytoskeleton. Sunderland, MA: Sinauer Associates Inc.

Isambert H, Venier P, Maggs AC, Fattoum A, Kassab R, Pantaloni D, Carlier MF. 1995. Flexibility of actin filaments derived from thermal fluctuations. Effect of bound nucleotide, phalloidin, and muscle regulatory proteins. J Biol Chem 270(19):11437–11444.

Ishikawa R, Sakamoto T, Ando T, Higashi-Fujime S, Kohama K. 2003. Polarized actin bundles formed by human fascin-1: their sliding and disassembly on myosin II and myosin V in vitro. J Neurochem 87(3):676–685.

Kabsch W, Mannherz HG, Suck D, Pai EF, Holmes KC. 1990. Atomic structure of the actin:DNase I complex [see comments]. Nature 347(6288):37–44.

Klinth J, Arner A, Mansson A. 2003. Cardiotonic bipyridine amrinone slows myosin-induced actin filament sliding at saturating [MgATP]. J Muscle Res Cell Motil 24(1):15–32.

Kozuka J, Yokota H, Arai Y, Ishii Y, Yanagida T. 2006. Dynamic polymorphism of single actin molecules in the actin filament. Nat Chem Biol 2(2):83–86.

Kozuka J, Yokota H, Arai Y, Ishii Y, Yanagida T. 2007. Dynamic polymorphism of actin as activation mechanism for cell motility. Biosystems 88(3):273–282.

Kraikivski P, Lipowsky R, Kierfeld J. 2006. Enhanced ordering of interacting filaments by molecular motors. Phys Rev Lett 96(25):258103.

Kron SJ, Spudich JA. 1986. Fluorescent actin-filaments move on myosin fixed to a glass-surface. Proc Natl Acad Sci USA 83(17): 6272–6276.

Kron SJ, Toyoshima YY, Uyeda TQ, Spudich JA. 1991. Assays for actin sliding movement over myosin-coated surfaces. Methods Enzymol 196:399–416.

Kumar S, ten Siethoff L, Persson M, Lard M, te Kronnie G, Linke H, Månsson A. 2012. Antibodies covalently immobilized on actin filaments for fast myosin driven analyte transport. PLOS One 7(10):e46298.

Kupi T, Grof P, Nyitrai M, Belagyi J. 2009. The uncoupling of the effects of formins on the local and global dynamics of actin filaments. Biophys J 96(7):2901–2911.

Lindberg U, Karlsson R, Lassing I, Schutt CE, Hoglund AS. 2008. The microfilament system and malignancy. Semin Cancer Biol 18(1):2–11.

Mucke N, Klenin K, Kirmse R, Bussiek M, Herrmann H, Hafner M, Langowski J. 2009. Filamentous biopolymers on surfaces: atomic force microscopy images compared with Brownian dynamics simulation of filament deposition. PLoS One 4(11):e7756.

Månsson A. 2012. Translational actomyosin research: fundamental insights and applications hand in hand. J Muscle Res Cell Motil 33(3–4):219–233.

Månsson A, Bunk R, Sundberg M, Montelius L. 2012. Self-organization of motor propelled cytoskeletal filaments at topographically defined borders. J Biomed Biotechnol 2012:647265.

Nitta T, Tanahashi A, Hirano M, Hess H. 2006. Simulating molecular shuttle movements: towards computer-aided design of nanoscale transport systems. Lab Chip 6(7):881–885.

Nitta T, Tanahashi A, Obara Y, Hirano M, Razumova M, Regnier M, Hess H. 2008. Comparing guiding track requirements for myosin- and kinesin-powered molecular shuttles. Nano Lett 8(8):2305–2309.

Oda T, Iwasa M, Aihara T, Maeda Y, Narita A. 2009. The nature of the globular- to fibrous-actin transition. Nature 457(7228):441–445.

Orlova A, Egelman EH. 1993. A conformational change in the actin subunit can change the flexibility of the actin filament. J Mol Biol 232(2):334–341.

Orlova A, Prochniewicz E, Egelman EH. 1995. Structural dynamics of F-actin: II. Cooperativity in structural transitions. J Mol Biol 245(5):598–607.

Ott A, Magnasco M, Simon A, Libchaber A. 1993. Measurement of the persistence length of polymerized actin using fluorescence microscopy. Phys Rev E: Stat Phys Plasmas Fluids Relat Interdisc Top 48(3):R1642–R1645.

Pampaloni F, Lattanzi G, Jonas A, Surrey T, Frey E, Florin EL. 2006. Thermal fluctuations of grafted microtubules provide evidence of a length-dependent persistence length. Proc Natl Acad Sci USA 103(27):10248–10253.

Pardee JD, Spudich JA. 1982. Purification of muscle actin. Methods Cell Biol 24:271–289.

Pavlov D, Muhlrad A, Cooper J, Wear M, Reisler E. 2007. Actin filament severing by cofilin. J Mol Biol 365(5):1350–1358.

Persson M, Gullberg M, Tolf C, Lindberg AM, Mansson A, Kocer A. 2013. Transportation of nanoscale cargoes by Myosin propelled actin filaments. PloS one 8(2):e55931.

Pollard TD, Borisy GG. 2003. Cellular motility driven by assembly and disassembly of actin filaments. Cell 112(4):453–465.

Prochniewicz E, Katayama E, Yanagida T, Thomas DD. 1993. Cooperativity in F-actin: chemical modifications of actin monomers affect the functional interactions of myosin with unmodified monomers in the same actin filament. Biophys J 65(1):113–123.

Prochniewicz E, Walseth TF, Thomas DD. 2004. Structural dynamics of actin during active interaction with myosin: different effects of weakly and strongly bound myosin heads. Biochemistry 43(33): 10642–10652.

Pyrpassopoulos S, Feeser EA, Mazerik JN, Tyska MJ, Ostap EM. 2012. Membrane-bound myo1c powers asymmetric motility of actin filaments. Curr Biol 22(18):1688–1692.

Rivetti C, Guthold M, Bustamante C. 1996. Scanning force microscopy of DNA deposited onto mica: equilibration versus kinetic trapping studied by statistical polymer chain analysis. J Mol Biol 264(5):919–932.

Steinmetz MO, Goldie KN, Aebi U. 1997. A correlative analysis of actin filament assembly, structure, and dynamics. J Cell Biol 138(3):559–574.

Sundberg M, Rosengren JP, Bunk R, Lindahl J, Nicholls IA, Tagerud S, Omling P, Montelius L, Mansson A. 2003. Silanized surfaces for in vitro studies of actomyosin function and nanotechnology applications. Anal Biochem 323(1):127–138.

Takatsuki H, Bengtsson E, Månsson A. 2013. Flexural rigidity of actin bundles propelled by heavy meromyosin. Biophys J 104(2): 649a.

Takatsuki H, Rice KM, Asano S, Day BS, Hino M, Oiwa K, Ishikawa R, Hiratsuka Y, Uyeda TQ, Kohama K, et al. 2010. Utilization of myosin and actin bundles for the transport of molecular cargo. Small 6(3):452–457.

Tokuraku K, Kurogi R, Toya R, Uyeda TQ. 2009. Novel mode of cooperative binding between myosin and Mg^{2+}-actin filaments in the presence of low concentrations of ATP. J Mol Biol 386(1):149–162.

Uyeda TQ, Iwadate Y, Umeki N, Nagasaki A, Yumura S. 2011. Stretching actin filaments within cells enhances their affinity for the myosin II motor domain. PloS one 6(10):e26200.

Van den Heuvel MG, de Graaff MP, Dekker C. 2008. Microtubule curvatures under perpendicular electric forces reveal a low persistence length. Proc Natl Acad Sci USA 105(23):7941–7946.

Vikhorev PG, Vikhoreva NN, Mansson A. 2008a. Bending flexibility of actin filaments during motor-induced sliding. Biophys J 95(12):5809–5819.

Vikhorev PG, Vikhoreva NN, Sundberg M, Balaz M, Albet-Torres N, Bunk R, Kvennefors A, Liljesson K, Nicholls IA, Nilsson L, et al. 2008b. Diffusion dynamics of motor-driven transport: gradient production and self-organization of surfaces. Langmuir 24(23): 13509–13517.

Yanagida T, Nakase M, Nishiyama K, Oosawa F. 1984. Direct observation of motion of single F-actin filaments in the presence of myosin. Nature 307(5946):58–60.

Yasuda R, Miyata H, Kinosita K. 1996. Direct measurement of the torsional rigidity of single actin filaments. J Mol Biol 263(2):227–236.